

Simultaneous Chandra, CSO and VLA Observations of Sgr A*: The Nature of Flaring Activity

F. Yusef-Zadeh¹, M. Wardle², C. Heinke³, C. D. Dowell⁴, D. Roberts¹, F. K. Baganoff⁵ &
W. D. Cotton⁶

ABSTRACT

Sgr A*, the massive black hole at the center of the Galaxy, varies in radio through X-ray emission on hourly time scales. The flare activity is thought to arise from the innermost region of an accretion flow onto Sgr A*. We present simultaneous light curves of Sgr A* in radio, sub-mm and X-rays that show a possible time delay of 110 ± 17 minutes between X-ray and $850 \mu\text{m}$ suggesting that the sub-mm flare emission is optically thick. At radio wavelengths, we detect time lags of 20.4 ± 6.8 , 30 ± 12 and 20 ± 6 minutes between the flare peaks observed at 13 and 7 mm (22 and 43 GHz) in three different epochs using the VLA. Linear polarization of $1 \pm 0.2\%$ and $0.7 \pm 0.1\%$ is detected at 7 and 13 mm, respectively, when averaged over the entire observation on 2006 July 17. A simple model of a bubble of synchrotron emitting electrons cooling via adiabatic expansion can explain the time delay between various wavelengths, the asymmetric shape of the light curves, and the observed polarization of the flare emission at 43 and 22 GHz. The derived physical quantities that characterize the emission give an expansion speed of $v_{exp} \sim 0.003 - 0.1c$, magnetic field of $B \sim 10-70$ Gauss and particle spectral index $p \sim 1-2$. These parameters suggest that the associated plasma cannot escape from Sgr A* unless it has a large bulk motion.

¹Department of Physics and Astronomy, Northwestern University, Evanston, IL 60208 (zadeh@northwestern.edu)

²Department of Physics, Macquarie University, Sydney NSW 2109, Australia (wardle@physics.mq.edu.au)

³Department of Astronomy, University of Virginia (coh5z@virginia.edu)

⁴Cal Tech, Jet Propulsion Laboratory, Pasadena, CA 91109 (cdd@submm.caltech.edu)

⁵Kavli Institute for Astrophysics and Space Research, MIT, Cambridge, MA 02139-4307 (fkb@space.mit.edu)

⁶National Radio Astronomy Observatory, 520 Edgemont Road, Charlottesville, VA 22903-2475 (bcotton@nrao.edu)

Subject headings: accretion, accretion disks — black hole physics — Galaxy: center

1. Introduction

Recent observations provide compelling evidence that the compact nonthermal radio source Sgr A* can be identified with a massive black hole at the center of the Galaxy. A major breakthrough in our understanding of this source came from stellar orbital measurements showing a mass $3\text{--}4 \times 10^6 M_\odot$ within 45 AU of the position of Sgr A* (e.g., Schödel et al. 2003; Ghez et al. 2004; Eisenhauer et al. 2005). This dark, massive object has been uniquely identified with the radio source Sgr A* through limits on the proper motion of the radio source, which show that Sgr A* must contain $> 4 \times 10^5 M_\odot$ and does not orbit another massive object (Reid & Brunthaler 2004).

A “sub-mm bump” was detected in the broad-band spectrum of Sgr A* (Zylka et al. 1995; Serabyn et al. 1997; Falcke et al. 1998); the sub-mm peak is thought to reflect the transition between optically thin emission at higher frequencies, and optically thick emission at lower frequencies. Observations of the time variability and polarization (Bower et al. 2005; Marrone et al. 2006; Macquart & Bower 2006; Yusef-Zadeh et al. 2007) are providing additional opportunities to study the innermost regions, within just a few Schwarzschild radii of the black hole event horizon, a region currently inaccessible via high spatial resolution imaging.

The energy radiated by Sgr A* is thought to be liberated from gas falling towards the black hole after being captured from the powerful winds of members of its neighboring cluster of massive stars (e.g., Melia 1992). The radiated power is several orders of magnitudes lower than expected, prompting a number of theoretical models to explain the very low efficiency (e.g., Melia & Falcke 2001; Yuan, Quataert & Narayan 2003; Goldston, Quataert & Tgumenshchev 2005; Liu & Melia 2001; Liu, Melia & Petrosian 2006). The spectrum of Sgr A* has been successfully modeled as a radiatively inefficient flow which is carried across the event horizon before radiating away its energy (Narayan et al. 1998). More recently, detection of radio and sub-millimeter polarization has allowed estimates of the integrated electron density in the accretion region from ~ 10 to 1000 Schwarzschild radii (Bower et al. 2003; Marrone et al. 2006). These estimates indicate much lower electron densities than predicted, implying that perhaps most of the material is not reaching the central black hole. Theoretical work (e.g., Yuan et al. 2003; Sharma et al. 2007) supports this picture, but leaves unanswered the question of whether infalling material finds itself in a convective flow (Narayan et al. 2002), a low-velocity outflow (Blandford & Begelman 1999, Igumenshchev

et al. 2003), or a fast jet (Yuan, Markoff & Falcke 2002). The frequency-dependence of the size of Sgr A* in the radio and sub-mm bands (e.g. Shen et al. 2005; Bower et al. 2006) suggests that the plasma responsible for the emission at these frequencies is not bound to the black hole but is escaping in a wind (Loeb & Waxman 2007).

Numerous multi-wavelength observations have studied Sgr A* in its flaring state. However, there are limited simultaneous observations able to measure the correlation of the variability of Sgr A* in different wavelength bands. (e.g., Eckart et al. 2004, 2006; Yusef-Zadeh et al. 2006a; Hornstein et al. 2007). A variety of mechanisms have been proposed to explain the origin of the variability in the NIR and X-rays (e.g., Melia & Falcke 2001; Yuan, Markoff & Falcke 2002; Liu & Melia 2002; Yuan, Quataert & Narayan 2003; Eckart et al. 2004, 2006; Goldston, Quataert & Igumenshchev 2005; Gillesen et al. 2006; Liu et al. 2006a,b). These studies imply that the NIR is synchrotron emission while the X-rays are most likely produced by synchrotron-self-Compton (SSC) or inverse Compton emission (Liu et al. 2004). Modelling of the processes responsible for heating and cooling the transient population of electrons responsible for the NIR and X-ray flares imply that it is produced in localised regions in the inner part of the accretion flow (Liu et al. 2006a,b; Bittner et al 2007).

The situation is less clear at sub-mm and radio frequencies where less dramatic short-term variability coexists with longer term variations presumably due to global changes in the accretion flow, and optical depth effects likely play a role in moderating the short-term variability (e.g. Goldston et al. 2005). Previous simultaneous near-IR and sub-mm measurements have shown two near-IR flares with durations of about 20–35 min within 2.5 hours of an 850 μm flare with an estimated duration of two hours (Yusef-Zadeh et al. 2006a). The first near-IR flare appeared to coincide with the submm flare whereas the second flare was delayed roughly by 160 minutes with respect to the submm flare. Two important points could be drawn: First, assuming that near-IR and submm flares are related to each other, this implies that the same synchrotron emitting electrons are responsible for production of both near-IR and sub-mm flares. The second point is that it is not clear whether the sub-mm flare is correlated simultaneously with the second bright near-IR flare, or is produced by the first near-IR flare but with a time delay of roughly 160 minutes. A delay between the peak emission in the near-IR and sub-mm suggests that the enhanced synchrotron emission in the compact region dominating the flaring emission is initially optically thick in the sub-mm, becoming optically thin due to expansion (van der Laan 1966).

To follow up this idea, we studied the light curves of Sgr A* at 7 and 13 mm taken in 2005. The light curves at both wavelengths show a 5-10% increase of flux with respect to their quiescent levels. We found that the emission at 13 mm may lag that at 7 mm by \sim

20 minutes, though with large uncertainty (Yusef-Zadeh et al. 2006b). To confirm the time delay between flares at successively longer wavelengths and to search for a time lag or other systematic correlation between other wavelength bands, we undertook a series of detailed observations using the VLA, CSO and *Chandra* telescopes.

This paper discusses the results of observations made on 2006 July 17 when all three telescopes participated in observing Sgr A* simultaneously. The Keck and SMA also joined the 2006 July 17 observation, and their results will be described in an accompanying paper (Marrone et al. 2007). We also present the results of short observations made on July 16, 2006 using the VLA and CSO, as well as the cross correlation of flare emission at 7 and 13 mm observed with the VLA on 2005 February 10 and 2006 February 10. Finally, fitting a simple adiabatically expanding plasma model gives reasonable matches to the light curve at two or more frequencies placing strong constraints on the physical parameters and size of the expanding plasma that are consistent with the parameters inferred for the accretion flow around Sgr A* and for the emission regions responsible for the NIR flares (Liu et al. 2006a,b; Bittner et al. 2007).

2. Radio, Submm and X-ray Observations

2.1. VLA Observations

Using the Very Large Array (VLA) of the National Radio Astronomy Observatory¹, we carried out observations in the B-array configuration on 2006 July 16 and 2006 July 17 for a total of 4 and 6 hours, respectively. Details of the total intensity and polarization calibration procedures observations are identical to previous measurements, as described in Yusef-Zadeh et al. (2007), with the exception that these observations used two sub-arrays simultaneously at 43 and 22 GHz. Thus, the measurements presented here are truly simultaneous in two observing bands. Two phase calibrators 1733-130 and 17444-31166 were employed. The VLA is undergoing an expansion and these observations used seven new Expanded (EVLA) antennas and 20 original (VLA) antennas. Because of higher and more variable amplitude gains of the EVLA antennas than the VLA antennas, we did not use any of the EVLA antennas in our analysis. Thus, on the average a total of eight to ten antennas are used in each sub-array. The light curves at 43 and 22 GHz have used uv -spacings longer than 100 $k\lambda$. We discarded data from antennas that showed large variation or high amplitude

¹The National Radio Astronomy Observatory is a facility of the National Science Foundation, operated under a cooperative agreement by Associated Universities, Inc.

gains during the run. All antennas had similar gain amplitude during the entire observation. The 43 GHz data on 2006 July 16 were noisy and could not be salvaged for time variability analysis. The light curve of the fast switching calibrator is obtained by calibrating it with the second calibrator 1733-130. Instrumental calibration was done in two steps, one for the entire period of observation and the other on a short time scale. We only used 17444-31166 for polarization calibration in both steps. A more detailed account of short time scale polarization calibration can be found in Yusef-Zadeh et al. (2007).

Two other observations made on 2005 February 10 and 2006 February 10 used the BnA and A+Pt array configurations of the VLA to study the time variability of Sgr A*. Both observations used fast switching techniques alternating between 43 and 22 GHz every few minutes. Early results including polarization results of these measurements are given in Yusef-Zadeh et al. (2006a, 2007). These observations used the same calibrators as in the July 2006 observations. These radio observations are different when compared with previous snapshot measurements (e.g., Zhao et al. 2004). First of all, the radio observations that have conducted in snapshot mode have no way of determining the flux stability of the complex gain calibrators. The 44 and 23 GHz observations are most affected by the opacity variability of the atmosphere. Unlike previous observations, we specifically used two nearby calibrators (one to independently calibrate the other) in a fast switching mode (30 on calibrator and 90 seconds on source) in order to make sure that the change in the flux of Sgr A* is not due to the atmospheric effects. These tests and techniques can not work when the data are taken in a snapshot mode. Even if the calibration is done correctly in a snapshot observing mode, and the observed variability is intrinsic to Sgr A*, it is not clear whether this is due to the change in the quiescent flux or true flaring activity. Lastly, the lack of simultaneous coverage make it difficult to claim time delays between peaks of emission in different wavelength bands.

2.2. CSO Observations

A $\sim 3'$ field surrounding Sgr A* was observed at $850 \mu\text{m}$ using the Caltech Submillimeter Observatory and the SHARC II camera (Dowell et al. 2003). The observations on 2006 July 16 began at 5:36 UT and ended at 10:50 UT, and the observations on 2006 July 17 began at 5:20 UT and ended at 10:21 UT. As was done in the past (Yusef-Zadeh al. 2006a), the field was observed with Lissajous scanning of the telescope with an amplitude of $\sim 100''$ and a period of ~ 20 seconds. The scanned observing permits an accurate measurement of all of the relative detector gains, and coverage of the surrounding dust emission allows the atmospheric transmission to be tracked better than using the CSO 225 GHz radiometer alone.

Absolute calibration was accomplished with observations of Callisto (13.6 Jy assumed)

and Neptune (27.5 Jy assumed), with an estimated uncertainty of 10%. At the 20'' resolution of CSO at 850 μm the emission of Sgr A* is somewhat confused with the emission from the surrounding molecular ring. We estimate an absolute uncertainty of 1 Jy in the flux of Sgr A* due to confusion, while noting that the accuracy of changes in flux is considerably better.

2.3. Chandra Observations

The imaging array of the Advanced CCD Imaging Spectrometer (ACIS-I; Garmire et al. 2003) on-board the *Chandra X-ray Observatory* (Wiesskopf et al. 2002) was used to observe Sgr A* simultaneously with the CSO and the VLA for 29.8 ks from 2006 July 17 04:15 to 12:37 (UT; ObsID 6363). ACIS-I was operated in timed exposure mode with detectors I0–3 and S2 turned on; the time between CCD frames was 3.141 s. The event data were telemetered in faint format. The data were analyzed using the *Chandra* Interactive Analysis of Observations (CIAO) version 3.3.0.1 and the calibration database version 3.2.2².

Figure 1 shows the (net) *Chandra*/ACIS-I lightcurve of Sgr A* in the 2–8 keV band obtained using a source aperture radius of 1''.5 and a surrounding sky annulus extending from 2'' to 4'', excluding regions around discrete sources and bright structures (see Baganoff et al. 2003). The bin size is 207.3 s. For more details about the *Chandra* data, see Marrone et al. (2007).

3. Results

Figure 1 shows a composite light curve of flaring activity in the X-ray (2–10 keV), 850 μm , 7 and 13 mm bands on 2006 July 17. The most interesting result of this multi-wavelength campaign is the detection of a strong X-ray and sub-mm flare. The 43 and 22 GHz light curves also show a relatively strong flare preceded by a weak flare near 4.25 UT at 43 GHz. The X-ray flare lasts for at least 90 minutes with a sharp rise and a slow decay having a peak X-ray luminosity of 4×10^{34} ergs s⁻¹ (Hornstein et al. 2007). The asymmetric profile of the 850 μm flare shows a slower rise and decay in its light curve than that of its X-ray counterpart. The duration of the submm flare is greater than 3.5 hours. The morphology, the duration and the time lag of the sub-mm flare with respect to the bright X-ray flare can all be understood in the context of expanding hot plasma (see §4). We also note a weak flare near 6h UT in the submm band with a peak flux of 200 mJy at 850 μm . This weak flare

²<http://cxc.harvard.edu/ciao>

was also detected at 1.2 mm based on simultaneous SMA observations during this campaign (Marrone et al. 2007).

Simultaneous near-IR observations on 2006 July 17 also detected a near-IR counterpart to the X-ray flare at K'-L' bands. However, near-IR observations started 36 minutes after the peak X-ray emission. In spite of incomplete time coverage in near-IR wavelengths, Hornstein et al. (2007) argue that the near-IR and X-ray flare emissions are associated with each other and simultaneous with no time delay.

3.1. Cross Correlation Study

3.1.1. 2006 July 17 and 2006 July 16

Our cross-correlations use the Z-transformed discrete correlation function algorithm (Alexander 1997; see also Edelson & Krolik 1988). This algorithm is particularly useful for analyzing sparse, unevenly sampled light curves. We identify the peak likelihood value, and a $1-\sigma$ confidence interval around that value, using a maximum likelihood calculation (Alexander 1997).

The top panel of Figure 2a shows the light curves of Sgr A* at $850\mu\text{m}$ and X-rays; the corresponding cross correlation peak is displayed in the bottom panel. Assuming that the two flares are related to each other, the cross correlation plot suggests that the sub-mm peak lags the X-ray peak by 110 ± 17 minutes. Also, assuming that the X-ray flare has a simultaneous near-IR counterpart, as Hornstein et al. (2007) suggest, the 110m time delay seen in Figure 2a is consistent with that observed between the near-IR and sub-mm peaks measured on 2004 September 4 (Yusef-Zadeh et al. 2006a). These time delay measurements imply that submm flare emission at $850\mu\text{m}$ is optically thick.

Figure 2b shows a cross-correlation peak between 7 and 13 mm emissions for the 2006 July 17 data. The maximum likelihood peak is 20.4 ± 6.8 minutes. The time lag between the 7 and 13 mm peak flare emission, as shown in Figure 2b, is consistent with a 20 minute time delay at these frequencies reported earlier (Yusef-Zadeh et al. 2006b).

We also performed a cross correlation analysis between the radio and submm flare emission of 2006 July 17 (Figure 3a). However, the strong flare emission in radio wavelengths occurs before the strong submm peak seen near 7:30h UT. There is a weak submm flare that is evident near 6h UT. This weak submm peak, which is clearly visible in the SMA light curve of 2006 July 17, has a better signal-to-noise at 1.3mm than at $850\mu\text{m}$ (Marrone et al. 2007). Due to the long duration and relatively high frequency of the radio and submm flares,

as well as the lack of simultaneous temporal coverage between VLA and CSO observations, the association of flares in radio and submm wavelengths is not clear. One possibility is that the strong 7 mm flare that peaks near 6:30-7h UT, as seen in Figure 1, is associated with the strong submm flare that peaks near 7:30h UT. The strong peak in the cross correlation plot in Figure 3a shows a negative time lag of ~ 1 hour for these two strong flares in radio and submm wavelengths. This result, however, implies that the strong submm peak is delayed with respect to the strong 7 mm peak by $66_{-1.8}^{+18}$ minutes. This is, of course, not consistent with the plasmon model of expanding plasma which predicts that low frequencies are delayed relative to high frequencies. On the other hand, Figure 3a also shows a weaker cross correlation peak with a positive time lag. Thus, we infer that the faint submm flare and quiescent emission with a peak flux of 2.7 Jy centered around 6h UT is likely to be associated with the strong 7 mm flare and quiescent emission with a peak flux of 1.7 Jy. This also suggests that both the X-ray and the strong submm flares are not related to the radio flares observed at 7 and 13mm. Given the uncertainty due to incomplete time coverage, the time lag between the weak 850 μm and 7 mm flares is estimated to be greater than 1.25 hours.

We also investigated the cross correlation of 850 μm data with 13 mm data taken on 2006 July 16. Figure 3b shows enhanced submm emission between 6:45h UT and 8:0h UT. Radio emission at 13 mm also shows the beginning of a flare between 7:30 and 8h UT. Again, the lack of simultaneous temporal coverage between VLA and CSO observations makes the cross correlation analysis quite uncertain. However, a peak is noted with a positive time lag in the bottom panel of Figure 3b. The delay between 850 μm and 13 mm is estimated to be roughly 65_{-23}^{+10} minutes. This time delay is consistent with the time lag noted with the 2006 July 17 cross correlation data, as shown in Figure 3a.

3.1.2. 2006 February 10 and 2005 February 10

We applied the cross correlation analysis to the 7 and 13 mm data taken on 2006 February 10 and on 2005 February 10 in the A-array plus Pie Town and the BnA hybrid configurations of the VLA, respectively (Yusef-Zadeh et al. 2006a, 2007). Figure 4a,b shows the cross correlation plots of 7 and 13 mm data corresponding to these observations. The 7 and 13 mm light curves from both observations are made based on uv data greater than 100 $k\lambda$. The maximum likelihood values with one σ error bar are 30 ± 12 and 20 ± 6 minutes for the 2006 February 10 and 2005 February 10 data, respectively. In both measurements, the strong peak indicates clearly that the 13 mm peak lags behind the 7 mm peak flare emission. Table 1 gives a summary of the time lag measured from cross correlating radio, submm and

X-ray data sets.

3.2. 43 and 22 GHz Polarization

The four panels of Figure 5a,b show the variation of the polarization plots at 7 and 13 mm, respectively, taken on 2006 July 17. The top three panels show the Stokes Q, U, and I whereas the bottom two panels show the degree of polarization and polarization angle. The data are binned every 20 minutes at both 7 and 13 mm. The average degree of polarization at 7 and 13 mm are $1\pm 0.2\%$ and $0.7\pm 0.1\%$, respectively.

We also obtained light curves of Stokes Q, U and I using 1733-130 instead of 17444-31166. We could not confirm the light curves of Stokes Q and U, as shown in Figure 5. We believe the reason for such a discrepancy is due to the residual instrumental errors of the calibrators as a function of elevation. If the residual errors are not taken out properly, they create different polarization light curves. We believe that 17444-31166 is a better polarization calibrator for this purpose as was observed every 90 seconds while tracking Sgr A* within 2° of its position. On the other hand, 1733-130 is observed once every 20minutes and is 16° away from from Sgr A*. It is possible that the stress due to gravity is responsible for not accounting properly for instrumental polarization correction as a function of time. Future observations with additional polarization calibrators are needed to confirm the low level of polarization we have reported here.

We note that both the degree of polarization and polarization angle tend to change during the flaring state when compared with those during the quiescent phase of Sgr A*. In particular, we note a possible increase in the degree of polarization to 2.5% and 1.5% at 7 and 13 mm, respectively. The polarization angle during the quiescent phase is close to 180 or 0 degrees at 7 and 13 mm, but a variation of about 100 degrees is detected during the flaring phase at both 7 and 13 mm. The average values of polarization angle at 7 and 13 mm during the flaring phase (i.e. > 6h UT) are estimated to be 106 and 87 degrees. The errors in the polarization angle for individual data points are obtained by taking the nominal Stokes Q and U values plus the derived $1-\sigma$ errors in the respective Stokes parameter to determine one limit in the polarization angle. The nominal Q and U values minus the $1-\sigma$ errors are used to determine the other limit relative to the nominal polarization. The polarization angle measurements correspond to a RM of -2.5×10^4 rad m^{-2} with no phase wrap; the RM estimate assumes the quadratic relationship between RM and the observed frequency. However, recent analysis of polarized emission from Sgr A* suggest that relativistic RM of polarized radiation should be considered (Ballantyne, Ozel, & Psaltis 2007; Yusef-Zadeh et al. 2007).

4. Modeling of sub-mm and radio flares

Models for the variable emission from Sgr A* have primarily focussed on the relationship between the dramatic flaring observed in the NIR and X-ray bands (Baganoff et al. 2003, Eckart et al. 2004, 2006; Yusef-Zadeh et al. 2006a; Hornstein et al. 2007). In these models the IR emission is produced by synchrotron emission from a transient population of near-GeV electrons in a $\sim 10\text{--}100$ G magnetic field, with the x-rays produced either by synchrotron from higher energy electrons (Yuan et al. 2003) or by inverse Compton scattering of either the sub-mm from the surroundings or directly associated with the transient population (ie synchrotron-self-Compton) (e.g. Yuan et al. 2003, 2004; Liu et al. 2004, 2006a,b). Scattering of NIR photons by the electrons responsible for the quiescent sub-mm emission may also contribute to the X-ray flux (Yusef-Zadeh et al. 2006). These models constrain the size of the emitting region to be a few Schwarzschild radii or less (Liu et al. 2004). The transient population of accelerated electrons may be produced via reconnection, acceleration in weak shocks (e.g. Yuan et al. 2003) or by heating by plasma waves (Liu et al. 2006a,b) driven by instabilities in the accretion flow or dissipation of magnetic turbulence. Detailed modelling of the latter process implies that the regions are compact suggesting that the flaring may be used to study the detailed evolution of the accelerated electron population in response to heating and radiative mechanisms (Bittner et al. 2007).

At lower frequencies, successive delays have been tentatively detected between flares at 350, 43 and 22 GHz (Yusef-Zadeh et al. 2006a), behaviour that is reminiscent of the emission from an adiabatically expanding synchrotron source that is initially optically thick, and becomes optically thin at successively lower frequencies as the source expands (cf. van der Laan 1966). This may reflect (for example) the expansion of a buoyant blob of synchrotron-emitting plasma created in a corona by a disk instability or a bright emission spot advected by an expanding wind in the vicinity of the black hole. Here we adopt a phenomenological approach focussed on the empirical behavior of the flares that is divorced from the uncertain global structure and dynamics of the outflow.

It turns out that this model matches the shapes of the profiles and the delay between frequencies surprisingly well, and that the derived emission region size, density and magnetic field strength are in broad agreement with the conditions inferred in global models of the accretion flow and in the detailed models for flaring in the NIR (Bittner et al. 2007).

Our earlier phenomenological modeling of the time delay assumed that at 350 GHz the flare emission was initially optically thin and showed that a steep energy spectrum ($\sim E^{-3}$) could explain the relative flux of the peak emission at lower, initially optically thick frequencies. Here we further test this model by applying it to the delayed flaring seen in the current observations. The presence of a possible 110-minute time delay between the peaks of

X-ray and 850 μm light curves suggests that the sub-mm flare emission may, in this case, be optically thick. Thus, here we investigate optically thick sub-mm and radio emission in the context of adiabatic expansion of hot plasma (van der Laan 1966) using different energy spectra of nonthermal particles. We also determine the physical parameters of the expanding blob models which then are used to model the polarization characteristics of the observed light curves in radio and submm wavelengths.

4.1. Time Delay as a Function of Spectral Index

The phenomenological model assumes that the flaring emission at sub-mm to radio frequencies is dominated by synchrotron emission from a compact expanding region filled with relativistic electrons with an energy spectrum $n(E) \propto E^{-p}$ threaded by a magnetic field. For simplicity, the particle density and spectrum and magnetic field strength are taken to be uniform. As the emitting region expands the magnetic field declines as R^{-2} because of flux-freezing, the energy of each relativistic particle declines as R^{-1} because of adiabatic cooling and the energy-integrated density of relativistic particles scales as R^{-3} . Following van der Laan (1966), the flux density scales as

$$S_\nu = S_0 \left(\frac{\nu}{\nu_0} \right)^{5/2} \left(\frac{R}{R_0} \right)^3 \frac{1 - \exp(-\tau_\nu)}{1 - \exp(-\tau_0)}, \quad (1)$$

where the synchrotron optical depth at frequency ν scales as

$$\tau_\nu = \tau_0 \left(\frac{\nu}{\nu_0} \right)^{-(p+4)/2} \left(\frac{R}{R_0} \right)^{-(2p+3)}. \quad (2)$$

Here τ_0 , the optical depth at which the flux density for any particular frequency peaks, depends only on p through the condition

$$e^{\tau_0} - (2p/3 + 1)\tau_0 - 1 = 0 \quad (3)$$

and ranges from 1 to 1.9 as p ranges from 1 to 3 (Yusef-Zadeh et al. 2006b). Thus given the particle energy spectral index p and the peak flux S_0 in the flaring component of the light curve at a reference frequency ν_0 , this model predicts the variation in flux density at any other frequency. A model for $R(t)$ is required to convert the dependence on radius to time: as a first approximation we adopt a simple linear expansion at constant speed v , so that $R = R_0 + v(t - t_0)$ where t_0 is the time of the peak flux at frequency ν_0 .

By way of illustration, we choose a peak flux $S_0 = 1.5 \text{ Jy}$ at $\nu_0 = 350 \text{ GHz}$, consistent with the observations presented here. Figure 6 shows the resulting light curves at sub-mm

and radio frequencies for particle energy indices $p = 2$ and 0.5 . This behaviour reflects the combined effects of adiabatic cooling and declining magnetic field, which imply that the *initial* energy of the electrons responsible for the peak emission increases as the plasma evolves. A flatter spectrum implies a relatively larger number of high energy particles at $t=0$, and therefore a greater expansion is required to cool them. The consequence of flattening the energy spectrum of particles is therefore to increase the time delay between peaks at various frequencies and to lengthen their durations.

4.2. Modeling the Light Curves

For a single frequency the functional form for a flare at one frequency uses one more parameter than a Gaussian fit (i.e. p and the expansion speed v , instead of the Gaussian FWHM), so that one expects a better fit than would be obtained with a gaussian, regardless of the merits of the model. Fortunately the contemporaneous light curves at other frequencies – including the delay time – are then fully determined without additional parameters. Therefore simultaneous light curves at two or more frequencies form a good test of the model.

The observables measured from a typical light curve at frequency ν_0 are the timing and magnitude of the peak flux (t_0 , and S_0), the particle index p and expansion speed in units of R_0 per unit time (which together determine the asymmetry and width of the flare), and the background level. The most uncertain of these is the value of the background, i.e. the quiescent flux, as this may slowly vary over the course of a flare.

The physical parameters of the emitting region are then determined as follows. The index p determines τ_0 , and so the value of S_0 fixes the radius R_0 via $S_0 = \pi R_0^2/d^2 \times (1 - \exp(-\tau_0))$ where d is the distance to the Galactic center. Then the expansion speed is determined in physical units. The determination of the magnetic field and electron density from the optical depth and size of the emitting region relies on assuming minimum and maximum energies (we adopt $E_{min} = 1$ MeV and $E_{max} = 100$ MeV, respectively) and equipartition between the magnetic field and relativistic electrons.

We do not perform maximum likelihood fitting given the phenomenological nature of the model, being content to achieve reasonable matches with the observed light curves. We modeled the sub-mm and radio light curves on 2006 July 17 and the radio data on 2005 February 10 and 2006 February 10. The model parameters are presented in Table 2.

The model for the submm light curve of 2006 July 17 is plotted as a solid line in Figure 7a. The sub-mm flare shows a slow decay and its asymmetric profile is fitted with a peak (excess) flux of 0.82 Jy at $850\mu\text{m}$ (350 GHz) at 7.65h UT. The particle spectral index $p=1$

(or $\alpha=1$), an expansion speed of $v = 0.0028c$ and a magnetic field of $B = 76$ G are derived from the fit. Note that the synchrotron cooling time for electrons emitting at 350 GHz is ~ 45 minutes, so that this may play a role in determining the decay of the light curve.

Separately from the submm data, the light curves of the radio flare that peak prior to the rise of the submm flare on 2006 July 17 are jointly fitted, as shown in Figure 7b. The peak flux of 0.23 Jy at 7 mm (43 GHz) at 6.55h UT is used to derive the value $p=1$, $v = 0.12c$ and a magnetic field of 11 G, as shown in Figure 7b. The quiescent flux was estimated to be 1 and 1.46 Jy at 22 and 43 GHz, respectively, with a spectral index of 0.58.

The model light curves of the 2005 February 10 data at 43 and 22 GHz are shown in Figure 8a. The derived quantities are $p=1.5$, $v=0.018c$ and $B=12$ G. We also derived the physical parameters of the flare emission for the 2006 February 10 observation. The light curve of this observation shows two overlapping flares on top of a fairly strong quiescent emission when compared to the flare emission observed on 2005 February 10. The fit to the light curve is shown in Figure 8b. The model uses peak flux of 300 and 240 mJy at 43 GHz centered at 14.3h and 16.3h UT for the first and second flare, respectively. The derived physical parameters for both flares are quite similar to each other (see Table 2) except that the value of particle energy index of the first flare ($p=1$) is flatter than that of the second flare ($p=2$).

4.3. Theoretical Polarization Curves

The parameters derived from modelling the variation in intensity can be used to compute the polarization properties of the transient emitting region, in other words to produce light curves in all four Stokes parameters I, Q, U and V. To illustrate this we compute the variations in Q and U for the physical parameters inferred of the emitting region inferred for the 2006 July 17 flare. To do this we use the analytic (but complicated!) solutions for the Stokes vector emerging from a homogeneous synchrotron-emitting sphere threaded by a uniform magnetic field given by Jones & O’Dell (1977).

The predicted polarization is sensitive to the assumption that the magnetic field in the emitting region is constant, as any spatial variation in B will tend to reduce the amplitude of the polarization. Indeed, we find that the model overpredicts the degree of polarization by a factor of around three, so for the purposes of illustration we reduce U and Q by this factor. Two additional parameters are needed to account for the orientation of the magnetic field to the line of sight: we find a reasonable match to U and Q at 43 GHz for a field lying in the plane of the sky with $PA= 20^\circ$. The quiescent emission at 43 GHz is linearly polarized

with $Q = -4$ mJy and $U = 6.6$ mJy, so we add these amounts to the model curves.

Figure 9 shows the fit to all Stokes parameters of the 43 and 22 GHz light curve of the 2006 July 17 flare. The match at 22 GHz is less compelling but despite the uncertainties, both in the data and the model, these results indicate the potential for improved measurements of polarization at multiple frequencies to severely test the emission model.

5. Discussion

The particle acceleration mechanism responsible for the NIR flaring associated with Sgr A* is not yet conclusively identified. Possibilities include acceleration in weak shocks (e.g. Yuan et al. 2003), magnetic reconnection events in a disc corona (e.g. Yuan et al. 2004) or acceleration by a spectrum of plasma waves associated with the dissipation of magnetically-driven turbulence (Liu et al. 2004; 2006a,b). Modelling of the NIR and X-ray flaring implies that the emission regions are compact, so that the flaring can be used to study the detailed evolution of the accelerated electron population in response to time-dependent heating and radiative mechanisms (Liu et al. 2006a,b; Bittner et al. 2007).

At the frequencies of interest here – below 350 GHz – we cannot directly investigate the mechanism responsible for the energization of the electrons because the flaring emission is optically thick and the synchrotron cooling time of the emitting particles is longer than the flare duration. However, the decaying part of the light curves are sensitive to the electron spectrum over a range of energies because a weakening magnetic field means that the energy of the electrons responsible for the synchrotron emission at a particular frequency increases with time; in addition adiabatic cooling of the particles implies that the electrons had an even higher energy at the onset of the flare. Adiabatic cooling in the absence of significant synchrotron losses implies that the energy of a particular electron scales as $1/R$, and the magnetic field strength scales as R^{-2} . Thus the energy of the electrons largely responsible for synchrotron emission at a particular frequency scales as R and their energy when the population was created scales as R^{-2} . Thus modelling of the flare profiles potentially tells us something of the initial accelerated population over about a factor of 5–10 in energy.

In our modelling we assumed for simplicity a power-law spectrum (E^{-p}) and inferred $p = 1-2$ for the asymmetric and more symmetric profiles of light curves, respectively. Fermi acceleration by a single adiabatic shock produces a power law energy distribution with $p \sim 2$ (e.g., Blandford and Eichler 1987). A harder particle spectrum can be produced if relativistic particles carry away a substantial fraction of the kinetic power of the shock (Drury & Völk 1981), or towards high energies by acceleration in multiple shocks (Melrose and Pope 1993;

Pope and Melrose 1994). Note, however, that many plausible models predict a relativistic Maxwellian by competition between accelerative and radiative processes (e.g. Bittner et al. 2007). It would therefore be of interest to compute the flaring at low frequencies assuming such spectra, but we leave that exercise to the future, noting that our inferred value of p may reflect the slope of the electron spectrum over a restricted range of energies.

The variation of energy index of particles may also have implications on the origin of the flaring component of X-ray emission. It has been argued previously that the X-ray counterparts to the near-IR flares are unlikely to be produced by synchrotron radiation in the typical ~ 10 G magnetic field for two reasons. First, emission at 10 keV would be produced by 100 GeV electrons, which have a synchrotron loss time of only 20 seconds, whereas individual X-ray flares rise and decay on much longer time scales (Baganoff et al. 2001). Second, the observed spectral index of the X-ray flares, $S_\nu \propto \nu^{-0.6}$ (Belanger et al. 2005), does not match the near-IR to X-ray spectral index of -1.35 ± 0.2 (Eckart et al. 2006). We favored an inverse Compton model for the X-ray emission, which naturally produces a strong correlation with the near-IR flares. In this picture, sub-millimeter photons are up-scattered to X-ray energies by the electrons responsible for the near-IR synchrotron radiation. In the inverse Compton scattering (ICS) picture, the spectral index of the near-IR flare must match that of the X-ray counterpart. The spectral indices of the X-ray and of the decaying part of the near-IR light curve on 2006 July 17 are estimated to be $\alpha = -0.3 \pm 0.6$ and -0.6 ± 0.2 , respectively, where $F_\nu \propto \nu^\alpha$ (Hornstein et al. 2007). These spectral indices are consistent within errors with the ICS picture. Hornstein et al. (2007) report a peak X-ray flux of 4×10^{34} ergs s $^{-1}$. In the ICS picture, the peak flux at K-band is estimated to be ~ 45 mJy assuming that the magnetic field is $B=20$ G and the near-IR spectral index $\alpha=-0.5$. The estimated near-IR flux depends on the submm source size and is assumed to have a radius of $3R_s$, which is quite uncertain.

The emission from the innermost region of Sgr A* can be divided into quiescent and flaring components. The quiescent flux dominates the emission at low energies (e.g., radio and submm wavelengths) whereas the flaring emission dominates in near-IR and X-ray wavelengths. Although a number of models have been proposed to explain the low luminosity of the quiescent flux and the origin of the flaring activity, the relationship between the quiescent and flaring states of Sgr A* is not fully understood. It is instructive to examine the relationship between these two components, The light curves shown in Figures 2 and 3 indicate clearly that the quiescent emission at 43 and 22 GHz varies on different days. The most dramatic increase of about 30% from 2005 February 10 to 2006 February 10 is noted. Figure 3 shows the quiescent emission of 2006, February 10 ranging between 2.2 and 2.3 Jy at 43 GHz whereas the light curve of Sgr A* a year earlier on 2005 February 10, shows a flux of ~ 1.65 Jy at the same frequency. Similar percentage daily changes can also be noted at 22 GHz. At sub-mm band, the 850 μ m (350 GHz) mean flux dropped by 1.5 Jy between

2005 July/August and 2006 July, This corresponds to a drop of 50% of the quiescent flux in 2006 July with a very high statistical error. This suggests that the emission at submm and radio wavelengths, like those in near-IR and X-rays could be mainly due to flaring activity and there is no true quiescent flux in the broad band spectrum of Sgr A*.

Thus, it appears that some similarities that can be drawn from comparing the broad band and flaring spectra of the quiescent flux of Sgr A*. One is the fact that sub-mm and radio emission is optically thick in both regimes. The peaks of both the broad band quiescent and flare spectra turnover somewhere in the sub-mm band. In addition, the fact that both quiescent and flare components vary in the optically and optically thin regions gives additional support to the idea that much of the quiescent emission could be due to flaring events. Near-IR light curves show that Sgr A* is active as much as 30% of the time. In the context of expanding hot plasma blobs, the variation of flux at optically thick submm and radio wavelengths may indeed be responsible for varying quiescent flux of Sgr A*. A more detailed study of the relationship between flaring and quiescent flux of Sgr A* should explore the possibility that much of the quiescent emission may be generated as a result of a sea of simultaneous low amplitude flare emission.

6. Concluding Remarks

In summary, the results presented here confirm the picture of expanding synchrotron emitting plasma as a number of observations in radio show evidence of time delay between the peaks of flare emission. The first evidence of a time delay between X-rays and 850 μm emission provides additional support for the optically thin near-IR/X-ray flare emission leading the optically thick sub-mm and radio flares by about 2-3 hours. In fact, this time delay clarified earlier simultaneous near-IR and sub-mm observations in 2004 that reported sub-mm flare lagging a near-IR flare by 160 minutes (Yusef-Zadeh et al. 2006a). The observed duration and the time delay of optically thick flare emission is consistent with the model.

The modeling of the light curves has given us a handle on a number of physical quantities associated with flaring activity including the initial magnetic field, the energy spectrum of the particles and the expansion speed, the magnetic field with a strength of 76 G derived from fitting optically thick submm light curve of 2006 July 17 is relatively high compared to the estimate of the magnetic field from model fitting of radio data. This high magnetic field corresponds to a synchrotron cooling time of 45 minutes in submm band, comparable to the decay of of the submm flares. This partially undermines the argument that dynamical cooling of submm flares must be important, because of the long synchrotron lifetime of

submm emitting electrons. Obviously, future correlation of submm and radio light curves are critical to examine the model and measure the initial magnetic field of the expanding plasma.

The suggestion that the emitting regions responsible for the flaring in the sub-mm and radio are undergoing expansion is consistent with the idea of a significant large scale outflow of the material associated with the sub-mm radio quiescent spectrum of Sgr A* (e.g. Loeb & Waxman 2007). Note, however, that our inferred expansion speeds need not correspond to the bulk velocity in the flow. Assuming that the bulk motion is large, then there may be some signature of outflowing material from Sgr A* although it is not clear if the outflowing material will be collimated as there is no definitive evidence that Sgr A* has a disk. Indeed, there are some hints that a collimated outflow may arise from Sgr A* in the past. For example, there is the intriguing radio continuum image of the inner few arcseconds of Sgr A* (Yusef-Zadeh, Morris & Ekers 1992). We speculate that these large-scale (10^{17} cm) blob-like structures could potentially be associated with a past outflow activity from Sgr A*.

We are grateful to Tal Alexander for the use of his ZDCF code. COH acknowledges the support of the Lindheimer Postdoctoral Fellowship. Research at the CSO is supported by the NSF under contract AST 0540882. F. K. B. received support for this work from NASA through *Chandra* Award Numbers G05-6093X and G06-7041X, issued by the *Chandra* X-ray Center under contract NAS8-03060, and SAO Award Number 2834-MIT-SAO-4018.

REFERENCES

- Alexander, T. 1997 in *Astronomical Time Series*, ed. D. Maoz, A. Sternberg & E. Leibowitz (Dordrecht:Kluwer), 163
- Baganoff, F. K., Bautz, M. W., Brandt, W. N., Chartas, G., Feigelson, E. D., Garmire, G. P., Maeda, Y., Morris, M., Ricker, G. R., Townsley, L. K. & Walter, F. 2001, *Nature*, 413, 45
- Baganoff, F. K., Maeda, Y., Morris, M., Bautz, M. W., Brandt, W. N., Cui, W., et al. 2003, *ApJ*, 591, 891
- Ballantyne, D. R., Ozel, F. & Psaltis, D. 2007, *ApJ*, 663, L17
- Bélanger, G., Goldwurm, A., Melia, F., Ferrando, P., Grosso, N., Porquet, D., Warwick, R. & Yusef-Zadeh, F. 2005, *ApJ*, 635, 1095

- Bittner, J. M., Liu, S., Fryer, C. L. & Petrosian, V. 2007, *ApJ*, 661, 863
- Blandford, R. D. & Begelman, M. C. 1999, *MNRAS*, 303, L1
- Blandford, R. & Eichler, D. 1987, *PhR*, 154, 1
- Bower, G. C. Falcke, H., Wright, M. C. & Backer, D. C. 2005, *ApJ*, 618, L29
- Bower, G. C., Wright, M. C. H., Falcke, H. & Backer, D. C. 2003, *ApJ*, 588, 331
- Drury, L. O. C. & Völk, J. H. 1981, *ApJ*, 248, 344
- Eckart, A., Baganoff, F. K., Morris, M., Bautz, M. W., Brandt, W. N., Garmire, G. P., Genzel, R., Ott, T., Ricker, G. R., Straubmeier, C., Viehmann, T., Schödel, R., Bower, G. C. & Goldston, J. E. 2004, *A&A*, 427, 1
- Eckart, A., Baganoff, F. K., Schoedel, R., Morris, M., Genzel, R., Bower, G. C., Marrone, D., Moran, J. M., Viehmann, T., Bautz, M. W., Brandt, W. N., Garmire, G. P., Ott, T., Trippe, S., Ricker, G. R., Straubmeier, C., Roberts, D. A., Yusef-Zadeh, F., Zhao, J. H. & Rao, R. 2006, *A&A*, 450, 535
- Edelson, R. A. & Krolik, J. H. 1988, *ApJ*, 333, 646
- Eisenhauer, F., Genzel, R., Alexander, T., Abuter, R., Paumard, T., Ott, T., Gilbert, A., Gillessen, S., Horrobin, M., Trippe, S., Bonnet, H., Dumas, C., Hubin, N., Kaufer, A., Kissler-Patig, M., Monnet, G., Ströbele, S., Szeifert, T., Eckart, A., Schödel, R. & Zucker, S. 2005, *ApJ*, 628, 246
- Falcke, H., Goss, W. M., Matsuo, H., Teuben, P., Zhao, Jun-Hui & Zylka, R. 1998, *ApJ*, 499, 731
- Falcke, H. & Markoff, S. 2000, *A&A*, 362, 113
- Garmire, G. P., Bautz, M. W., Ford, P. G., Nousek, J. A., Ricker, G. R., Jr. 2003, *SPIE*, 4851, 28G
- Ghez, A. M., Wright, S. A., Matthews, K., Thompson, D., Le Mignant, D., Tanner, A., Hornstein, S. D., Morris, M., Becklin, E. E. & Soifer, B. T. 2004, *ApJ*, 601, L159
- Gillessen, S., Eisenhauer, F., Quataert, E., Genzel, R., Paumard, T., Trippe, S., Ott, T., Abuter, R., Eckart, A., Lagage, P. O., Lehnert, M. D., Tacconi, L. J. & Martins, F. 2006, *ApJ*, 640, L163
- Goldston, J. E., Quataert, E. & Igumenshchev, I. V. 2005, *ApJ*, 621, 785

- Igumenshchev, I. V., Narayan, R. & Abramowicz, M. A. 2003, *ApJ*, 592, 1042
- Jones, T. W. & O’Dell, S.L. 1977, *ApJ*, 214, 522
- Hornstein, S. D., Matthews, K., Ghez, A. M., Lu, J. R., Morris, M., Becklin, E. E., Rafelski, M. & Baganoff, F. K. 2007, *ApJ*, 667, 900
- Liu, S. & Melia, F. 2001, *ApJ*, 561, L77
- Liu, S. & Melia, F. 2002, *ApJ*, 573, L23
- Liu, S., Petrosian, V. & Melia, F. 2004, *ApJ*, 611, L101
- Liu, S., Melia, F. & Petrosian, V. 2006a, *ApJ*, 636, 798
- Liu, S., Petrosian, V., Melia, F. & Fryer, C. L. 2006b, *ApJ*, 648, 1020
- Macquart, J. P. & Bower, G. C. 2006, *ApJ*, 641, 302
- Marrone, D. P., Moran, J. M., Zhao, J.-H. & Rao, R. 2006, *ApJ*, 640, 308
- Marrone, D. P., Baganoff, F. K., Morris, M., Moran, J. M., Ghez, A. M., Hornstein, S. D., Dowell, C. D., Munoz, D. J., Bautz, M. W., Ricker, G. R., Brandt, W. N., Garmire, G. P., Lu, J. R., Matthews, K., Zhao, J.-H., Rao, R. & Bower, G. C. 2007, *ApJ*, submitted
- Mauerhan, J. C., Morris, M., Walter, F. & Baganoff, F.K. 2005, *ApJ*, 623, L25
- Melia, F. 1992 *ApJ*, 387, L25
- Melia, F. & Falcke, H. 2001, *ARA&A*, 39, 309
- Melrose, D. B. & Pope, M. H. 1993, *PASA*, 10, 222
- Miyazaki, A., Tsutsumi, T. & Tsuboi, M. 2004, *ApJ*, 611, L97
- Narayan, R., Mahadevan, R., Grindlay, J. E., Popham, R. G. & Gammie, C. 1998, *ApJ*, 492, 554
- Pope, M. H. & Melrose, D. B. 1994, *PASA*, 11, 175
- Reid, M. J. & Brunthaler, A. 2004, *ApJ*, 616, 872
- Schödel, R., Ott, T., Genzel, R., Eckart, R. D., Mouawad, N. & Alexander, T. 2003, *ApJ*, 596, 1015

- Serabyn, E., Carlstrom, J., Lay, O., Lis, D. C., Hunter, T. R., Lacy, J.H. & Hills, R. E. 1997, ApJ, 490, L77
- Sharma, P., Quataert, E. & Stone, J. M. 2007, ApJ, in press
- Shen, Z.-Q., Lo, K. Y., Liang, M.-C., Ho, P. T. P. & Zhao, J.-H. 2005, Nature, 438, 62
- van der Laan, H. 1966, Nature, 211, 1131
- Weisskopf, M. C., Brinkman, B., Canizares, C., Garmire, G., Murray, S. & Van Speybroeck, L. P. 2002, PASP, 114, 1
- Yuan, F., Markoff, S. & Falcke, H. 2002, A&A, 383, 854
- Yuan, F., Quataert, E. & Narayan, R. 2003, ApJ, 598, 301
- Yuan, F., Quataert, E. & Narayan, R. 2004, ApJ, 606, 894
- Yusef-Zadeh, F., Bushouse, H., Dowell, C. D., Wardle, M., Roberts, D., Heinke, C., Bower, G. C., Vila-Vilar, B., Shapiro, S., Goldwurm, A., Belanger, G., 2006a, ApJ, 644, 198
- Yusef-Zadeh, F., Morris, M. & Ekers, R. D. 1990, Nature, 348, 45
- Yusef-Zadeh, F., Roberts, D., Wardle, M., Heinke, C. O. & Bower, G. C. 2006b, ApJ, 650, 189
- Yusef-Zadeh, F., Wardle, M., Cotton, W. D., Heinke, C. O. & Roberts, D. A. 2007, ApJ, 668, L47
- Zylka, R., Mezger, P.G., Ward-Thompson, D., Duschl, W. J. & Lesch, H. 1995, A&A, 297, 83
- Zhao, J.-H., Herrnstein, R. M., Bower, G. C., Goss, W. M. & Liu, S.M. 2004, ApJ, 603, L85

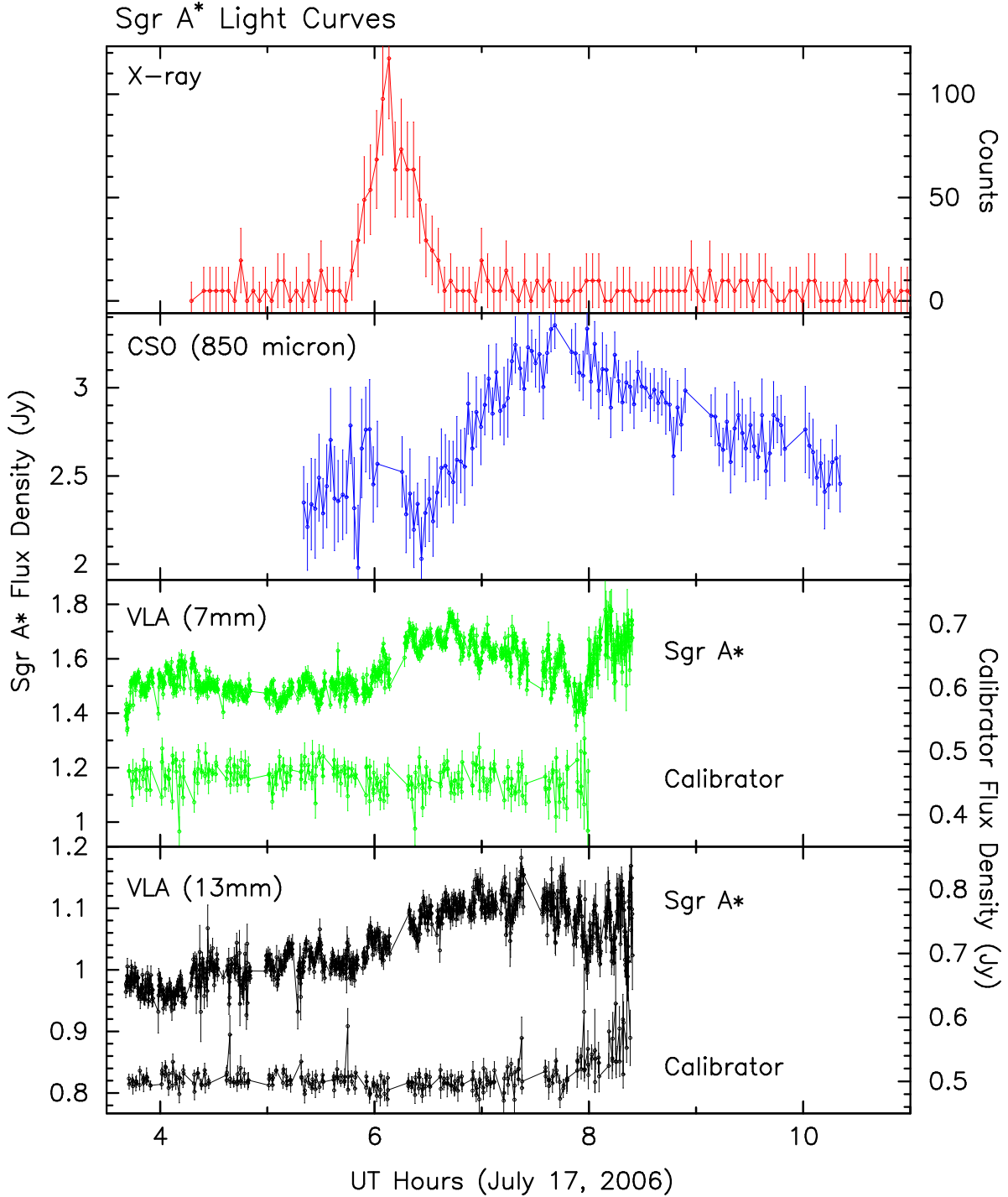


Fig. 1.— The light curves of Sgr A* is shown during the 2006 July 17 observing campaign in four different panels using *Chandra*, CSO and VLA observatories. The fluxes are measured in Jy except for the X-ray data which are shown as a count rate. The X-ray (2-8 keV), submm (850 μm) and radio (7 and 13 mm) data are binned every 207 seconds, 20 minutes and 9 seconds, respectively. The light curves of the phase calibrator 17444-31166 are also presented at 7 and 13 mm in the bottom two panels. Note that the flux increase at 7mm near 8.2h UT is likely to be due atmospheric errors at low elevation.

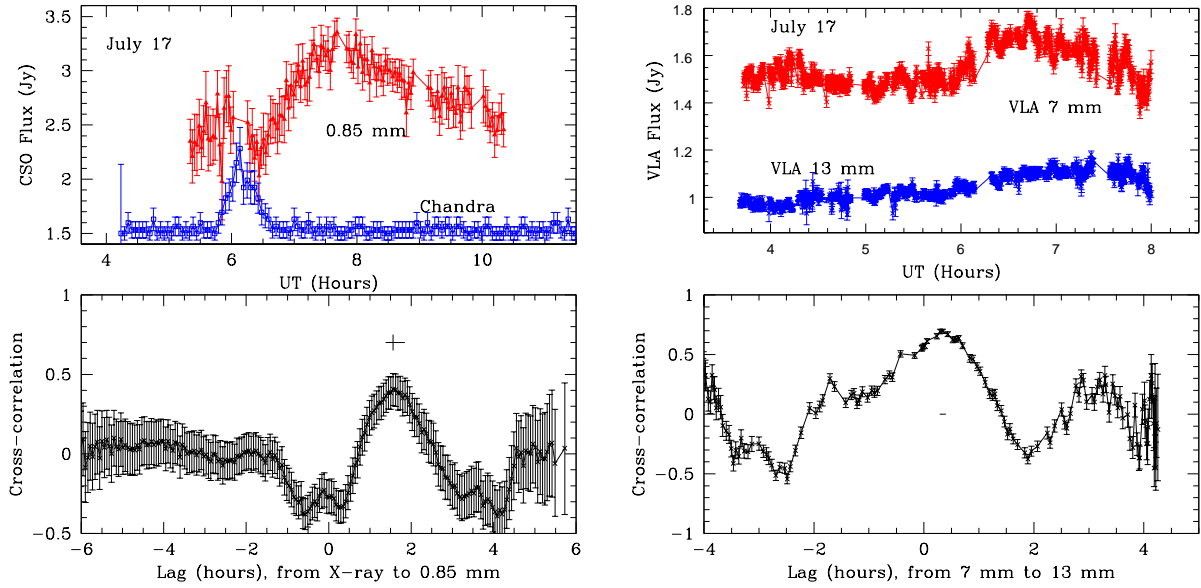


Fig. 2.— **(a) Left** the light curves of X-ray and submm emission and the corresponding cross correlation plot showing a time lag 110 ± 17 minutes. **(b) Right** The cross correlation and light curves of 7 and 13 mm emission with a time lag of 20.4 ± 6.8 minutes. The maximum likelihood peak with a $1\text{-}\sigma$ error bar, is shown in the bottom panels of each figure.

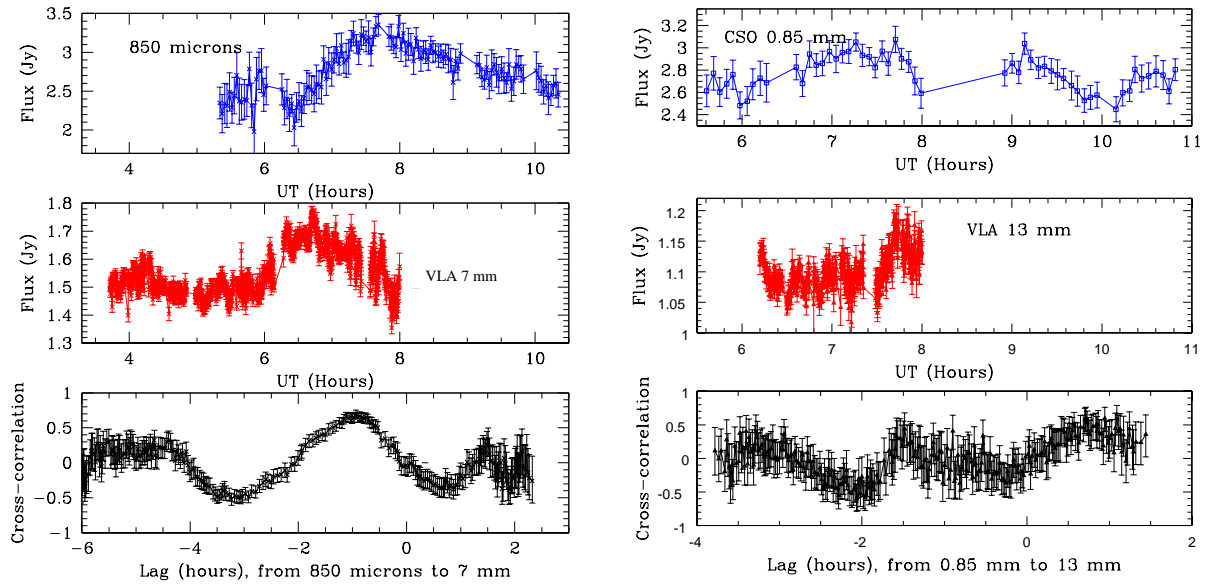


Fig. 3.— **(a) Left** Light curves of $850\mu\text{m}$ (blue color) and 7 mm (red color) emission on 2006 July 17 and the corresponding cross correlation plot. The cross correlation plot shows radio emission peak lags behind the weak submm peak emission near 6h UT by 1.25 hours. **(b) Right** Light curves of $850\mu\text{m}$ or 0.85 mm (blue color) and 13 mm (red color) flare emission on July 16, 2006 and the corresponding cross correlation plot. Both plots show that the peak radio emission lags behind the submm peak by $45\pm 30\text{m}$.

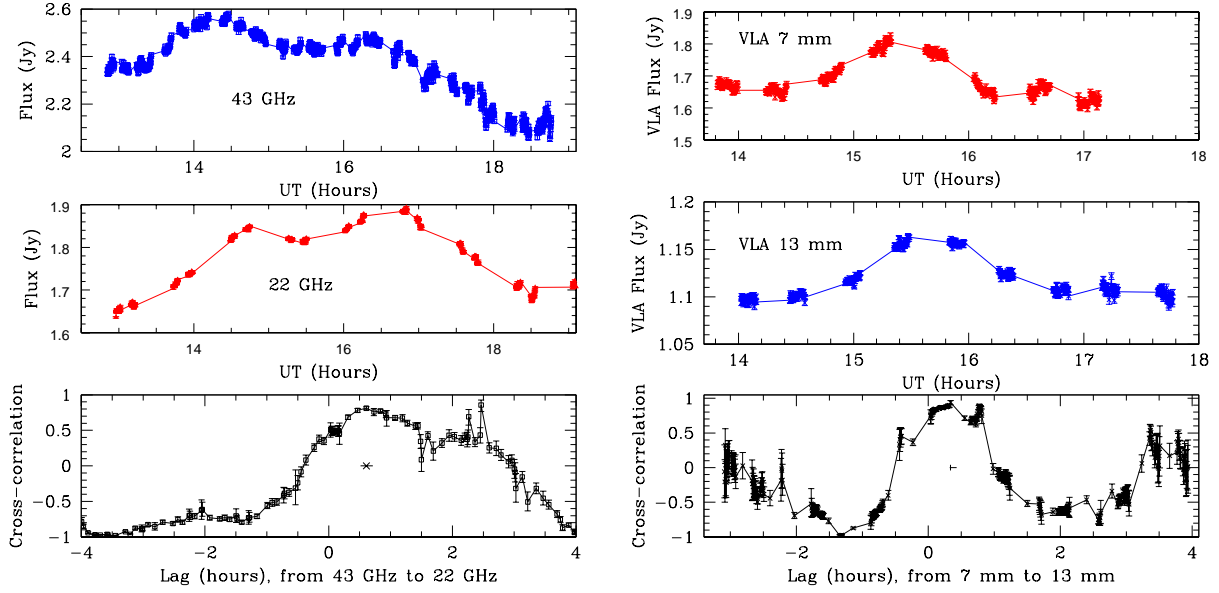


Fig. 4.— **(a) Left** Light curves of 7mm (43 GHz) and 13 mm (22 GHz) flare emission on 2006 February 10 and the corresponding cross correlation plot in the bottom panel. The 13 mm peaks show a time lag of 20.4 ± 6.8 minutes with respect to 7 mm peaks. **(b) Right** Similar to (a) except the data is based on 2005 February 10 data. The time lag is estimated to be 30 ± 12 minutes. The maximum likelihood peak, identified as a star with a $1\text{-}\sigma$ error bar, is shown in each figure. The parameters of the cross correlation peak can be found in Table 1.

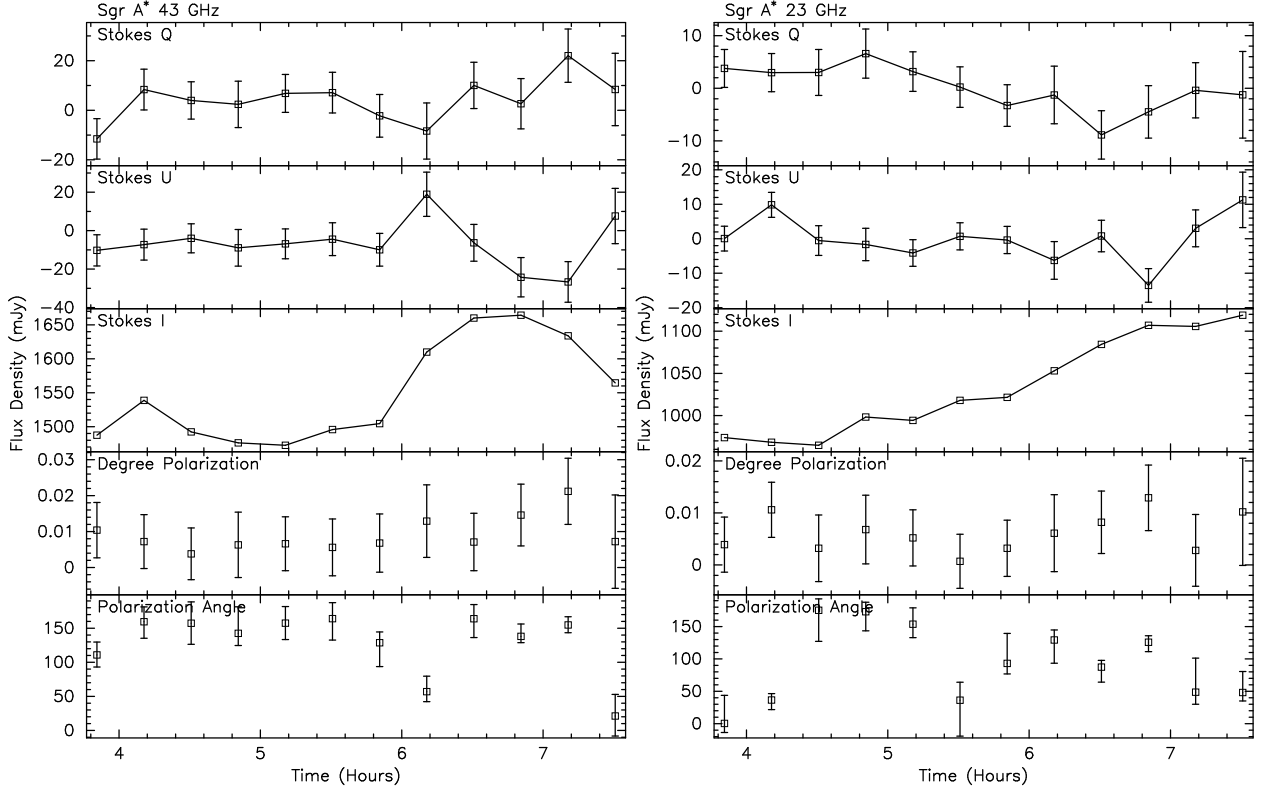


Fig. 5.— **(a) Left** The light curves of Stokes Q, U, I, the degree of polarization and the polarization angle at 7 mm. **(b) Right** Similar to (a) except at 13 mm. The time interval sampled at 7 and 13 mm are 1200 seconds.

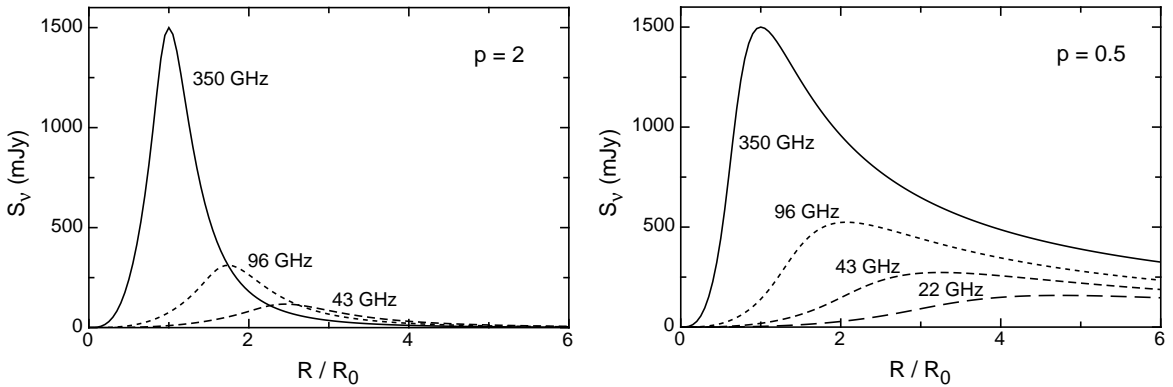


Fig. 6.— **(a) Left** Theoretical light curve of Stokes I for optically thick synchrotron emission at submm and radio frequencies as a function of expanding blob radius. These light curves assume a energy power law index $p=2$. **(b) Right** Similar to (a) except that the particle spectrum is flat with $p=0.5$. Note the long decay time of the light curve as the spectrum flattens.

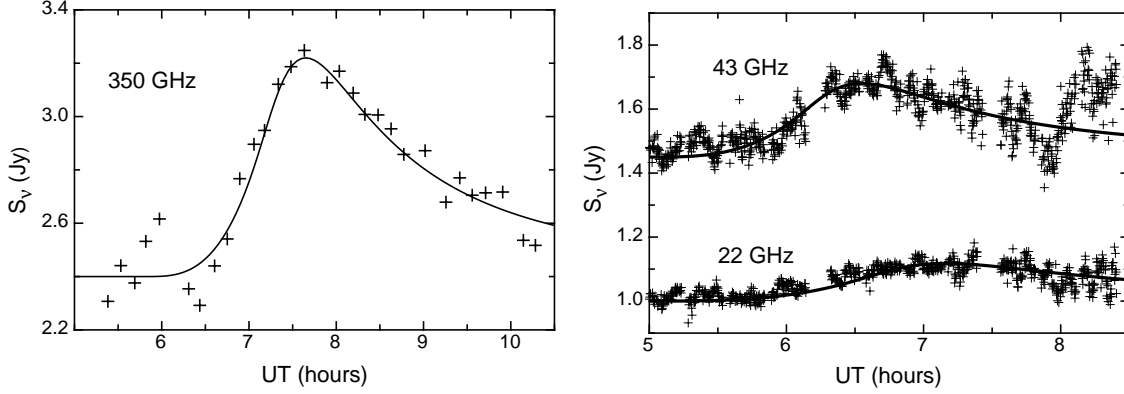


Fig. 7.— **(a) Left** The solid line represents a model fitting the sub-mm light curve on 2006 July 17 at 350 GHz. Note that the fit is made only to the light curve of the bright flare and not to the weak flare peaking around 6h UT. **(b) Right** Similar to (a) except that the 43 and 22 GHz light curves are fitted simultaneously for the 2006 July 17 data. The parameters of the 2006 July 17 fits for both the sub-mm and radio light curves can be found in Table 2.

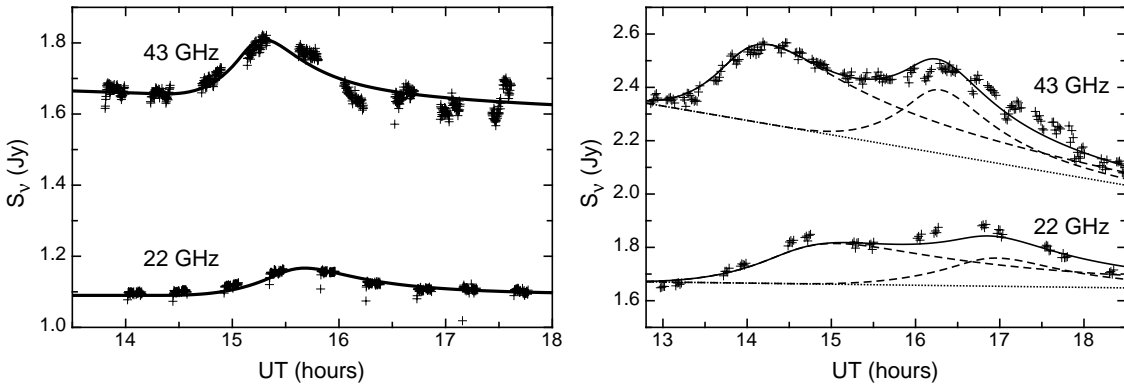


Fig. 8.— **(a) Left** Similar to Figure 7 except that the light curve of a single flare at 43 and 22 GHz are fitted simultaneously. The data is taken on 2005 February 10. **(b) Right** Similar to (a) except that the light curves of two overlapping flares on 2006 February are fitted simultaneously at 43 and 22 GHz. The parameters of the fits to the 2005, February 10 and 2006 February 10 light curves can be found in Table 2 .

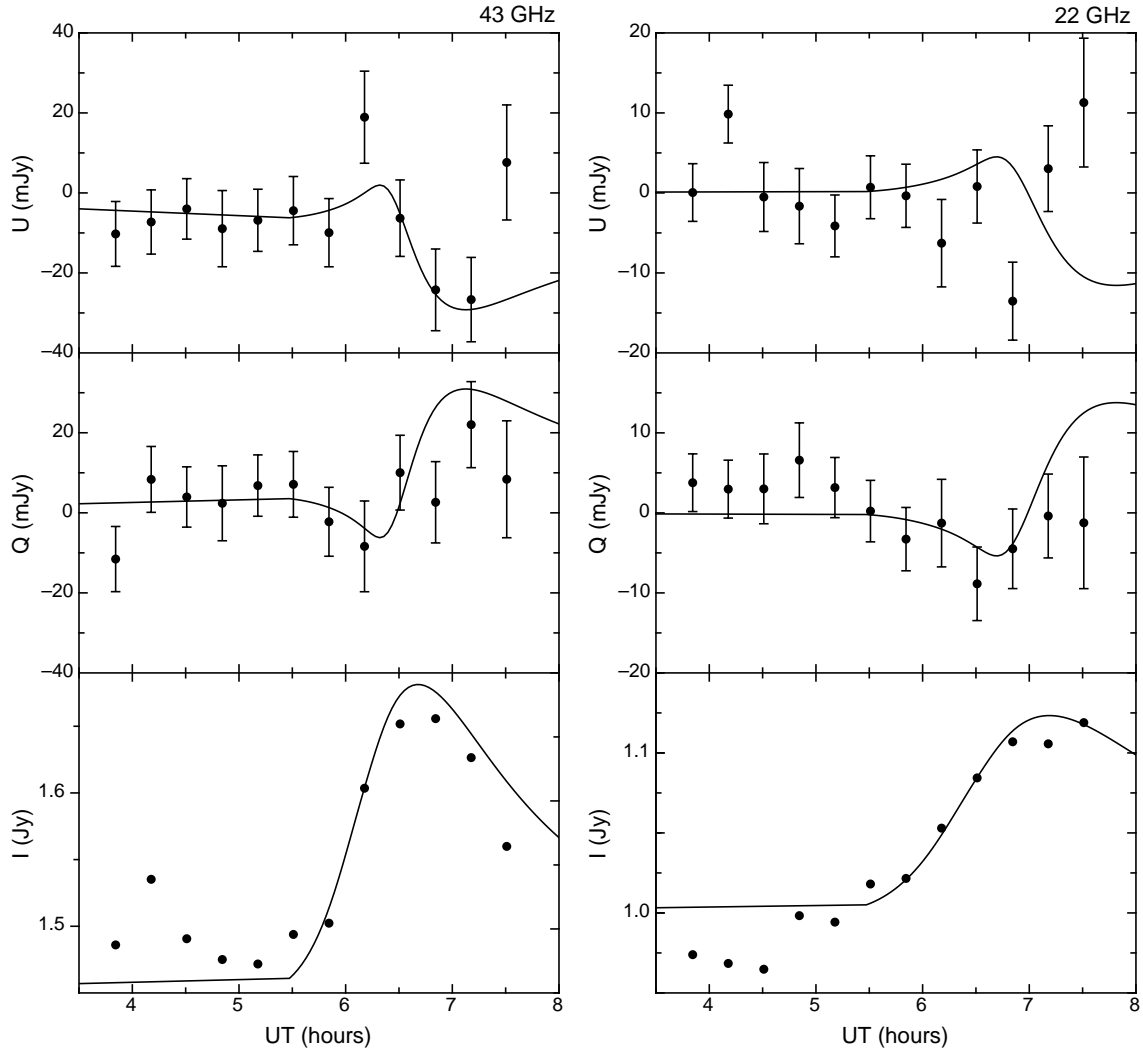


Fig. 9.— (a) **Left** The light curves of IQU Stokes on 2006 July 17 at 43 GHz are shown in three panels. The solid curves show simultaneous fit to the light curves using the expanding plasmon model. (b) **Right** Similar to (a) except at 22 GHz

Table 1. Measured Peak Fluxes and Time Lags

Date	Peak flux				Time Delay		
	7mm (Jy)	13mm (Jy)	850 μ m (Jy)	X-ray (erg s ⁻¹)	X-ray–850 μ m (min)	7mm–13mm (min)	850 μ m–13mm (min)
2006 July 17	1.76	1.2	3.35	4 \times 10 ³⁴	110 \pm 17	20.4 \pm 6.8	—
2006 July 16	—	1.2	3.09	—	—	—	65 ⁺¹⁰ ₋₂₃
2005 Feb 10	1.76	1.15	—	—	—	30 \pm 12	—
2006 Feb 10	2.6	1.76	—	—	—	20 \pm 6	—
2006 Feb 10	2.5	1.80	—	—	—	20 \pm 6	—

Table 2. Fitted Parameters to the Light Curves

Date	Quiescent Flux Jy	Background subtracted peak flux			Particle Index p	Expansion Speed v/c	Initial B (Gauss)	Initial Radius (R _s)
		7mm (mJy)	13mm (mJy)	850 μ m (mJy)				
2005 Feb 10	1.62–1.64	160	—	—	1.5	0.018	12	1.9
"	1.09	—	75	—	1.5	0.018	12	1.9
2006 Feb 10	2.06	300	—	—	1	0.013	10.7	2.5
"	2.33	240	—	—	2	0.016	10.4	3.2
"	1.65	—	150	—	1	0.013	10.7	2.5
"	1.67	—	110	—	2	0.016	10.4	3.2
2006 July 17	1.45	230	—	—	1	0.15	11	2.2
"	1.0	—	120	—	"	"	"	"
"	2.40	—	—	820	1	0.0028	76	0.50